MAGNETIC RESONANCE IN MEDICINE 17, 197–212 (1991)

Quantitative Measurement of Tissue Perfusion and Diffusion *in Vivo*

THOMAS L. CHENEVERT,[1] JAMES G. PIPE, DAVID M. WILLIAMS, AND JAMES A. BRUNBERG

Department of Radiology, University of Michigan Medical Center, 1500 East Medical Center Drive, Ann Arbor, Michigan 48109

Received October 24, 1989; revised February 13, 1990

Magnetic resonance imaging techniques designed for sensitivity to microscopic motions of water diffusion and blood flow in the capillary network are also exceptionally sensitive to bulk motion properties of the tissue, which may lead to contrast artifact and large quantitative errors. The magnitude of bulk motion error that exists in human brain perfusion/diffusion imaging and the inability of cardiac gating to adequately control this motion are demonstrated by direct measurement of phase stability of voxels localized in the brain. Two methods are introduced to reduce bulk motion phase error. The first, a postprocessing phase correction algorithm, reduces coarse phase error but is inadequate by itself for quantitative perfusion/diffusion MRI. The second method employs orthogonal slice selection gradients to define a column of tissue in the object, from which echoes may be combined in a phase-insensitive manner to measure more reliably the targeted signal attenuation. Applying this acquisition technique and a simplistic model of perfusion and diffusion signal attenuations yields an estimated perfusion fraction of 3.4 ± 1.1% and diffusion coefficient of $1.1 \pm 0.2 \times 10^{-5}$ cm^2/s in the white matter of one normal volunteer. Successful separation of perfusion and diffusion effects by this technique is supported in a dynamic study of calf muscle. Periods of normal blood flow, low flow, and reactive hyperemia are clearly distinguished in the quantitative perfusion results, whereas measured diffusion remained nearly constant.

INTRODUCTION

Techniques for the *in vivo* determination of tissue water diffusion coefficients may hold significant clinical relevance in characterizing disease processes and tissue types, although this is an area that has yet to be widely explored clinically. The same is true, perhaps to greater extent, for measurement of tissue perfusion by MRI. These techniques would be valuable, for example, in the evaluation of disorders in the central nervous system related to vascular disease, trauma, and perinatal asphyxia. Other applications include grading ischemic states, vascularity of tumors or vascular malformations, and quantifying tissue response to vasoactive agents.

The ability of magnetic resonance to accurately determine diffusion coefficients of isolated samples using the pulsed field gradients is established (*1*, *2*). Similar techniques have also been incorporated within MRI formats (*3–6*). Ideally, the MRI methods can be utilized to display the combined effects of all intravoxel incoherent motions (IVIM) (*3*), or the individual contributions of perfusion flow in capillaries (*7*) which

[1] To whom requests for reprints should be addressed.

0740-3194/91 $3.00

mimic diffusion, and diffusion itself. The successful extension of diffusion measurement methods to *in vivo* imaging is, however, not straightforward. The quality of results depends heavily on system performance, cardiac gate parameters, and the individual being scanned (*4*, *8*, *9*). Results are often unsatisfactory with ghost artifacts obscuring image detail. Presence of ghost artifact, whether related to system instability or patient motion, is clear evidence of signal loss unrelated to incoherent motion. Signal averaging may mask the artifact but does not restore lost signal. Consequently, the true nature of signal loss and the degree to which coherent bulk motion effects or instabilities contribute to the apparent IVIM contrast are unknown (*4*). The topic of meaningful quantification of perfusion and diffusion values from *in vivo* data is perhaps even more controversial.

The first objective of this work is to demonstrate the degree to which IVIM imaging of the human brain is compromised by bulk tissue motions. The second objective is to achieve significant improvement in perfusion/diffusion quantification via different acquisition and processing procedures. Two methods are introduced toward this end: (1) a phase correction algorithm to mitigate bulk motion and system instability effects, and (2) limited volume selection which may be used alone for one-dimensional imaging or in combination with the phase correction algorithm for two-dimensional imaging. Limited data on measurements of normal human brain and calf muscle are presented herein. These results are intended to demonstrate feasibility of quantitative isolation of perfusion and diffusion effects *in vivo*, but are otherwise not verified due to lack of direct comparison with other experimental methods.

THEORY

NMR signal attenuation due to molecular self-diffusion in the presence of field gradients is given by

$$S_b = S_0 e^{-Db} \qquad [1]$$

where S_b and S_0 are the signal amplitudes acquired with and without motion sensitization gradients applied, respectively, D is the diffusion coefficient, and b describes the motion sensitization field gradient waveform. In this study the waveform consists of two rectangular pulses of amplitude G straddling a 180 rf pulse. Each gradient pulse has duration δ with their leading edges separated by Δ so that (*1*)

$$b = (\gamma G\delta)^2[\Delta - \delta/3]. \qquad [2]$$

In biological systems diffusion is more appropriately modeled as restricted diffusion within the permeable cellular structure. The reader is referred elsewhere (*2*, *10*) for more detailed accounts of restricted diffusion; in this discussion we simply refer to the measured property as "diffusion" and realize its value is dependent on measurement time scale.

In vivo systems have additional motions to consider. These include large (multivoxel) vessel blood flow, CSF flow, perfusion flow in the capillary network, and bulk tissue motion due to cardiac pulsation, respiration, and muscular movement. Consider for a moment only perfusion flow. Its motion may also be modeled as incoherent because of indeterminate flow direction and the large number of capillaries (*11*) coexisting

within an MRI voxel. Use of the model of Le Bihan *et al.* (*3*), Eq. [1] can be expanded to include perfusion effects:

$$S_b = S_0[(1 - f) + Ff]e^{-Db}, \quad [3]$$

where f is the fraction of signal in S_0 attributable to flowing blood within capillaries, and F is an attenuation factor of the blood signal due to motion dephasing. For the set of gradient factors, b, employed in these experiments, the dephasing of flow is considered complete ($F \approx 0$) for nonzero b, whereas $F \approx 1$ when $b = 0$. Since capillary blood volume is only a few percent of the total tissue volume (*12*) one can show (*3*)

$$\ln(S_0/S_b) \cong f + Db. \quad [4]$$

Consequently, slope and intercept of $\ln(S_0/S_b)$ as a function of b correspond to diffusion and blood signal fraction, respectively. However, it should be emphasized that while the blood signal fraction f is measurable via perfusion dynamics, it is distinct from true perfusion, which is usually expressed as volume flow rate per gram of tissue. Also, it should be noted that for f to represent the volume fraction of flowing blood and not just the signal fraction, differences in diffusion and relaxation properties between blood and surrounding tissues should be negligible. These caveats, while noteworthy, are not the main source of controversy nor key impediments to *in vivo* perfusion/diffusion MRI and quantification. Therefore, for brevity in this report we shall refer to f as "perfusion" or "perfusion fraction."

Diffusion coefficients of soft tissue and body fluid specimens are on the order of 10^{-5} cm^2/s (*2*, *3*, *10*, *13*). Sensitivity to such microscopic motions requires gradient factors of 10^4 s/cm^2 or greater to impart adequate incoherent motion attenuation to the signal. Accompanying the high gradient factor is a high phase shift per unit velocity, which for the waveform described above is given by (*14*)

$$\Phi_v = \gamma G \delta \Delta. \quad [5]$$

Herein lies a major challenge to quantitative perfusion/diffusion measurement *in vivo* since relatively minor bulk tissue motions produce major phase shifts. If these phase shifts are not reproduced throughout the MRI scan, coherent phase cancellation amidst signal averaging and phase encoding reconstruction overwhelm, or at least greatly compromise, accurate quantification of incoherent perfusion/diffusion processes (*4*). For example, using the phase shift values of Table 1, one can see that the bulk motion speed of a given voxel must be reproducible to approximately ± 75 μm/s during the scan to maintain phase stability of $\pm 20°$. In addition, system instabilities aggravated by strong gradient pulses may also produce phase shifts yielding attenuation unrelated to the subject.

Correction Algorithm for Coherent Phase Shifts

The undesired phase shifts discussed above can be modeled as follows. Nonaveraged spin echoes with motion sensitization gradients (i.e., $b \neq 0$) give rise to an NMR signal

TABLE 1

Motion Sensitization Gradient Parameters

Lable	Amplitude (G/cm)	Phase shift per unit velocity[a] (degrees/mm/s)	b^a (s/cm^2)
*b*0	0	0	0
*b*1	0.464	129	7,702
*b*2	0.696	194	17,327
*b*3	0.95	265	32,300

[a] Gradient timing parameters: δ = 36 ms, Δ = 50.6 ms.

$$\mathbf{S}_b(k_x, k_y) = \int S_b(x, y) e^{i\Phi_{k_y}(x,y)} e^{i2\pi(k_x x + k_y y)} dxdy, \quad [6]$$

where k_x and k_y are frequency and phase encoding variables; $\Phi_{k_y}(x, y)$ is an arbitrarily large, spatially dependent phase error that varies with each k_y; $\mathbf{S}_b$ are the actual acquired data; and S_b are the data if acquired free of phase errors. That is, bulk motion and system-related phase shifts are allowed to vary unpredictably for each phase encoding line. If Φ_{k_y} is independent of y, then the Fourier transform with respect to k_x yields

$$\mathbf{S}_b(x, k_y) = S_b(x, k_y) e^{i\Phi_{k_y}(x)}. \quad [7]$$

In addition, if there is minimal y dependence of the change in object contrast due to perfusion and diffusion attenuation relative to the original object contrast (i.e., *b*0 image), then the phase of $S_0(x, k_y)$ is an approximation of the phase of $S_b(x, k_y)$. That is, the collective perfusion and diffusion effects are modeled as pure attenuation, $\alpha(x)$, of $S_0(x, k_y)$, whereas all phase errors are embodied in $\Phi_{k_y}(x)$:

$$\mathbf{S}_b(x, k_y) \cong S_0(x, k_y) e^{-\alpha(x)} e^{i\Phi_{k_y}(x)}. \quad [8]$$

Phase correction is achieved by creating a data set having the magnitude of $\mathbf{S}_b(x, k_y)$ and the phase of the motion-insensitive data $S_0(x, k_y)$:

$$\mathbf{S}'_b(x, k_y) = |S_b(x, k_y)| \frac{S_0(x, k_y)}{|S_0(x, k_y)|}. \quad [9]$$

Now that the random phase shifts with respect to k_y are removed, the second Fourier transform is applied to $\mathbf{S}'_b$ followed by magnitude calculation of image intensity, I_b. Finally, a pixel-by-pixel linear fit of $\ln(I_0/I_b)$ versus b yields perfusion and diffusion images.

Limited Volume Acquisition

Although phase errors are allowed to be arbitrarily large and variable with respect to x and time (i.e., each phase encoding line), the assumption that all observed phase differences between $S_0(x, k_y)$ and $S_b(x, k_y)$ are independent of y and originate from

undesired processes is fairly restrictive. Validity of these assumptions will vary with body region scanned and choice of phase and frequency encoding axes. Based on measurements described below, the assumptions will often be invalid, or at least lead to uncertain results, when imaging the human brain. However, if one collects only signals from a volume of tissue where the assumptions are valid locally, then quantitative accuracy can be improved. This localization may be achieved by two-dimensional selective rf pulse schemes (*15*) or, as done in this work, orthogonal slice-selective 90° and 180° rf pulses to define a sensitive column in the object (*16*, *17*). The selected column has full frequency encoding dimension and resolution but limited slice and phase encoding dimension. If phase encoding is not applied, individual echoes from the selected column may be Fourier transformed, magnitude calculated, then averaged to produce a one-dimensional image at each motion sensitization gradient setting for subsequent calculation of quantitative one-dimensional perfusion and diffusion images of the selected tissue column. If phase encoding is used, the phase correction algorithm may be applied to produce two-dimensional perfusion and diffusion images of the selected column.

MATERIALS AND METHODS

Experiments were performed on a 1.5-T clinical scanner (General Electric Medical Systems, Milwaukee WI) using the sequence shown in Fig. 1, with all postprocessing performed on a VAX 11/750 computer (Digital Equipment Corp., Maynard MA). Except for G_{motion}, gradient waveforms were designed to be temporally compact to reduce first- and second-moment dephasing of flow signal in the motion-insensitive ($b0$) acquisition. For simplicity, only G_{motion} was used in the calculation of b. The design of the other gradient pulses minimized their impact on IVIM attenuation. For example, the effective b of the G_{180} waveform was less than 1% of the weakest, nonzero G_{motion} b value. Theoretically, a minimum of three b settings is required to calculate both perfusion and diffusion; however, in these experiments four b values were used as outlined Table 1. The four gradient settings were applied in an interleaved fashion along the superior/inferior direction. Assignment of G_{180}, G_{ph}, G_{frq}, and postprocessing routines was varied to address several distinct experimental objectives.

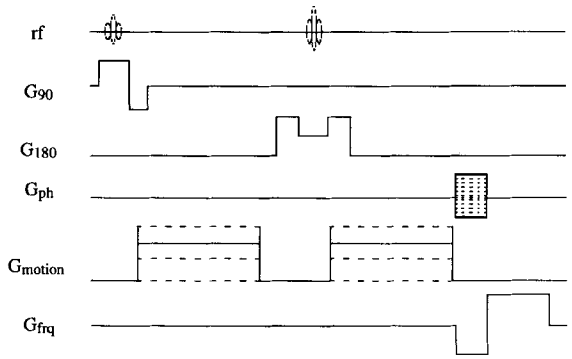

FIG. 1. Spin-echo sequence having optional phase encoding and optional orthogonal slice selection for limited volume acquisition. Motion sensitization gradients are interleaved and usually colinear with G_{frq}.

Temporal Phase Stability via Cardiac Gating in Human Brain Studies

This experiment was designed to demonstrate the degree of bulk motion phase instability in perfusion/diffusion imaging of the human brain and to determine whether cardiac gating provides adequate motion control. A 10 × 10-mm column of tissue was defined in the brain along the $z(S/I)$ direction via G_{90} on $y(A/P)$, G_{180} on $x(R/L)$, and G_{frq} on z. No phase encoding was applied; rather, 128 single excitation echoes at each b setting were collected with cardiac gating (TR = 2 ECG periods, trigger delay = 300 ms) and without gating (TR = 1.5 s). The column was offset 25 mm to the right of midline such that an area free of CSF could be analyzed. Following 1D FT, the phase of a 10 × 10 × 1.9-mm voxel located in the white matter was plotted as a function of echo number to demonstrate bulk motion reproducibility with and without gating at the high motion sensitivity gradient setting ($b3$). A static gel phantom was scanned under similar conditions to document system stability, since instabilities can mimic motion artifact.

Perfusion and Diffusion Imaging and Quantification of the Human Brain

Coronal brain imaging was performed with frequency encoding and motion sensitization gradients applied along z to minimize undesired phase variation in the phase encoding direction. Full field-of-view data sets were acquired using interleaved b values with ECG gating (TR = 2 ECG periods, trigger delay = 300 ms, TE = 99 ms, 10-mm slice, single excitation, 128 matrix) and without gating (TR = 2 s, other parameters unchanged). The nonzero b data sets were phase corrected, as outlined above, then used for pixel-by-pixel calculation of slope (diffusion) and intercept (perfusion fraction) of $\ln(I_0/I_b)$ as a function of b. Pixels having values outside an acceptable range ($0\% < f < 100\%$ or $0 < D < 20 \times 10^{-5}$ cm^2/s) or having associated data below a noise threshold were redefined as zero for display purposes.

In limited volume scans, data from selected 10 × 10-mm tissue columns (G_{90} on y, G_{180} on x, and G_{frq} on z along S/I direction) were acquired using interleaved b values. In one case, phase encoding was applied to demonstrate location of the column (TR = 2 s). As with the full field-of-view situations, phase correction of the nonzero b data was required for subsequent perfusion/diffusion image calculations of the selected column. Separate non-phase-encoded limited volume data sets were collected with cardiac gating (TR = 2 ECG periods, trigger delay = 300 ms) and without gating (TR = 1.5 s). Phase-encoded and non-phase-encoded data were nonaveraged and 128 echos were collected at each b setting such that total acquisition time was 4 × 128 × TR. Phase corrections were not required for non-phase-encoded data since echoes were combined following Fourier transform and magnitude calculation. One-dimensional quantitative images of perfusion and diffusion were then produced by a linear fit of $\ln(I_0/I_b)$ vs b.

Perfusion and Diffusion Quantification of Variable Flow to Calf Muscle

To provide supportive evidence that calculated diffusion and perfusion fraction values are derived from distinct aspects of signal attenuation, and that so-called perfusion fraction is truly related to blood flow, the following experiment was performed.

Axial gradient recalled echo imaging was performed to identify major vessels in the calf to target a 30 × 30-mm column of tissue (long axis along the S/I direction) having both a region free of major vessels and another containing major vessels. Orthogonal slice selection of this column was used in acquisition of non-phase-encoded, nongated, 128 single-excitation echoes, TR = 2 s, at each interleaved b value. The total scan time of 18 min was divided into three equal periods: the first-period blood flow to the calf was normal; during the second period a pressure cuff around the thigh was inflated to 200 mm to stop most flow to the calf; and for the remaining 6 min the cuff was deflated to allow reflow to the calf. After Fourier transform and magnitude calculation, only 21 echoes at each b value (i.e., approximately 3-min worth of data) were combined independently from each period to produce quantitative 1D perfusion and diffusion images of the calf before, during, and after pressure cuff application. Specifically, data from 3-min windows just prior to cuff application, the latter half of cuff application, and immediately after cuff release were analyzed.

RESULTS AND DISCUSSION

Figure 2 displays results of the temporal phase stability experiment with and without cardiac gating. The time courses of phase of a 10 × 10 × 1.9-mm voxel within the brain of a normal volunteer measured at high motion sensitivity (i.e., $b3$ setting) is shown for nongated (Fig. 2a) and cardiac-gated (Fig. 2b) acquisitions. As expected, the large first moment of the motion sensitization gradient produces extreme phase

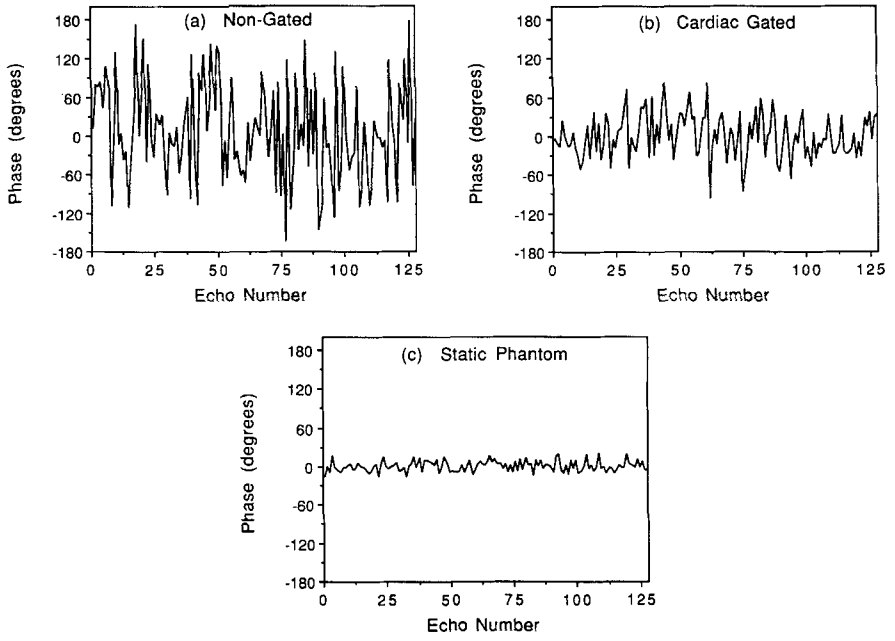

FIG. 2. Temporal phase stability when motion sensitization gradient is applied. Phase time courses of a voxel in the brain measured (a) without cardiac gating, (b) with cardiac gating, and (c) in a static phantom to demonstrate system stability.

variability in the nongated data due to bulk motion. Cardiac gating provides some improvement but, overall, is inadequate for reproducing all phase shifts. This is due to asynchronous motions such as respiration or irregular cardiac motion. Although results may vary for different subjects, different regions in the brain, and different ECG gating delays, the severity of phase variation indicates there would be probable contamination of incoherent motion quantification estimates by coherent motion processes when echoes are combined in a phase-sensitive manner within signal averaging or 2D FT reconstruction. Furthermore, location of this voxel indicates the brain itself, not just CSF, undergoes significant bulk motion. The existence of brain motion has been demonstrated by others (*17*). This implies that elimination of the CSF signal by exceptionally high b values is not a solution to bulk motion artifacts (*18*). The stable phase of the static phantom (Fig. 2c) indicates the most of the random phase in the human experiment is not due to system instability. The standard deviations of phase for the human and phantom motion-insensitive data ($b0$) were less than 6°.

Figure 3 displays coronal images of the brain acquired at $b0$ (Fig. 3a) and $b3$ settings reconstructed without phase correction (Fig. 3b) and following phase correction (Fig. 3c). Phase correction yields significant motion artifact reduction; however, the calculated perfusion (Fig. 3d) and diffusion (Fig. 3e) images, aside from being signal to noise limited, still display residual artifact due to regional phase disparity. That is, the model that tissues on a common phase encoding direction line move together is not strictly satisfied. The effects of this incorrect assumption are clearly demonstrated by the impact of the static phantom at the FOV periphery. Phase encoding was horizontal in this acquisition; therefore, the static phantom which has anomalous phase relative to pulsatile brain tissue projects an artifact horizontally through tissue. While present in Figs. 3c and d, the artifact is best visualized in the diffusion image (Fig. 3e) as indicated by the arrows. In a separate experiment, G_{90}, G_{180}, and G_{frq} were applied along y, z, and x, respectively, to define a right-to-left oriented 10 × 10-mm column in the brain through the ventricles. With phase encoding not applied, the spatial phase variability along the column could be inspected directly. Not surprisingly, results showed the ventricles to be most discordant in phase relative to surrounding brain. Of greater interest were the peak phase variations within the solid brain matter. These were observed to be as high as 180° between central and peripheral brain. We expect this spatial phase variability to be a major contributor to the asymmetries in the images shown in Figs. 3d and e.

Cardiac gating noticeably improves quality of the motion-sensitive image (Fig. 4b), in general agreement with the temporal phase stability experiment described above. However, significant asymmetries persist in subsequent calculated perfusion (Fig. 4c) and diffusion (Fig. 4d) images. These asymmetries, seen as increased intensity on the left side of images (right side of brain), are presumably artifactual since this is a normal volunteer. The phase-corrected versions of images in Figs. 4b–d are shown in Figs. 4e–g. While some improvements are evident, highly dynamic regions, such as the ventricles and suprasellar and perichiasmatic cistern regions in the brain, still produce artifacts, even after gating and phase correction. These artifacts are commonly observed for blood flow in large vessels and pulsatile CSF in ventricles. In fact, while the flow in large vessels and ventricles may be nonuniform, it is also macroscopic and nonrandom; therefore, the perfusion/diffusion model of Eq. [3] is not well suited.

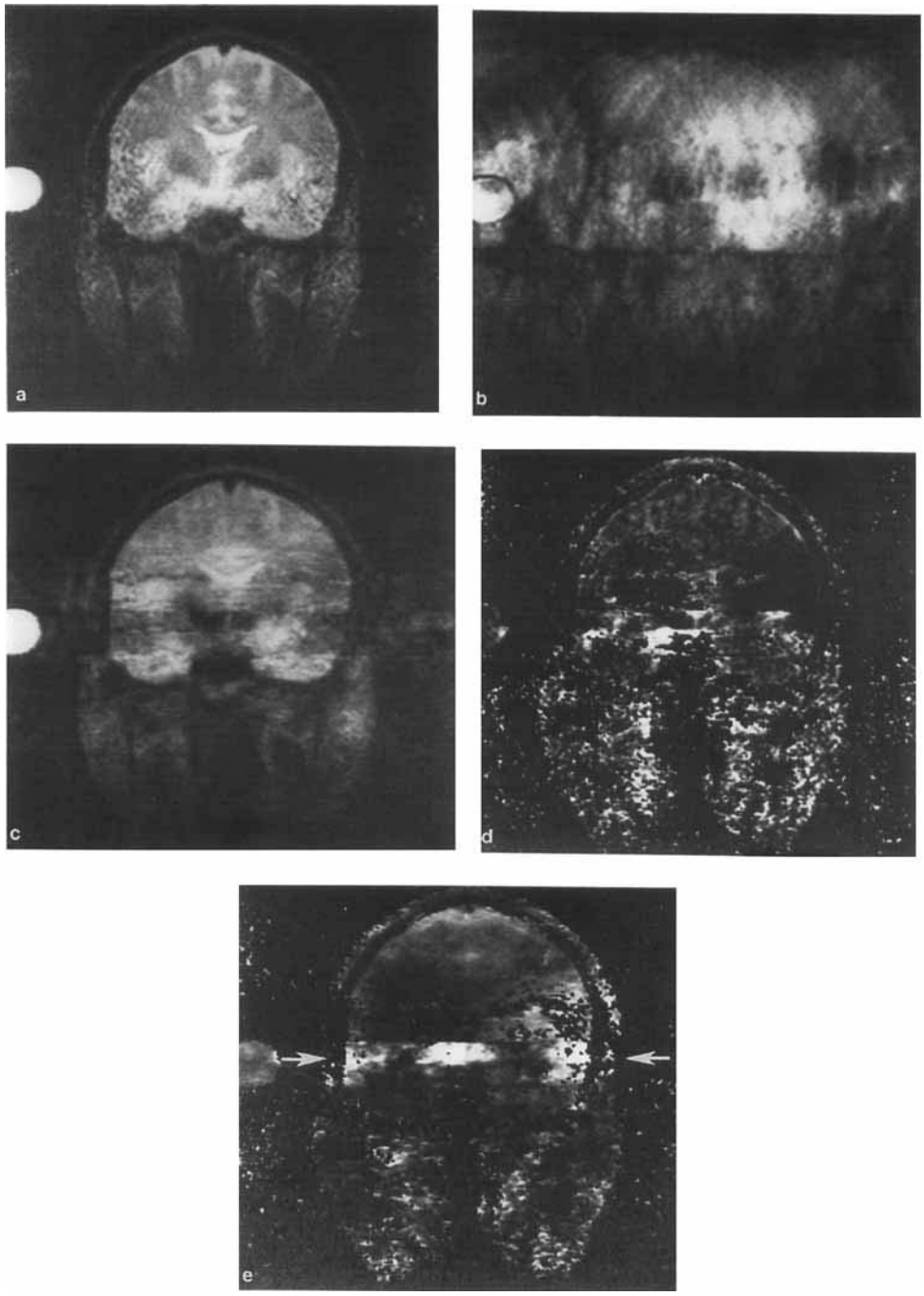

FIG. 3. Coronal images of the brain without cardiac gating acquired with (a) low motion sensitivity (i.e., *b*0); (b) high motion sensitivity (i.e., *b*3) without phase correction; and (c) high motion sensitivity with phase correction. Calculated (d) perfusion and (e) diffusion images from phase-corrected data sets. Arrows in (e) indicate phase artifact projected from the static phantom on the left-hand side of the image. The phantom/tissue phase discrepancy violates an assumption of the correction algorithm.

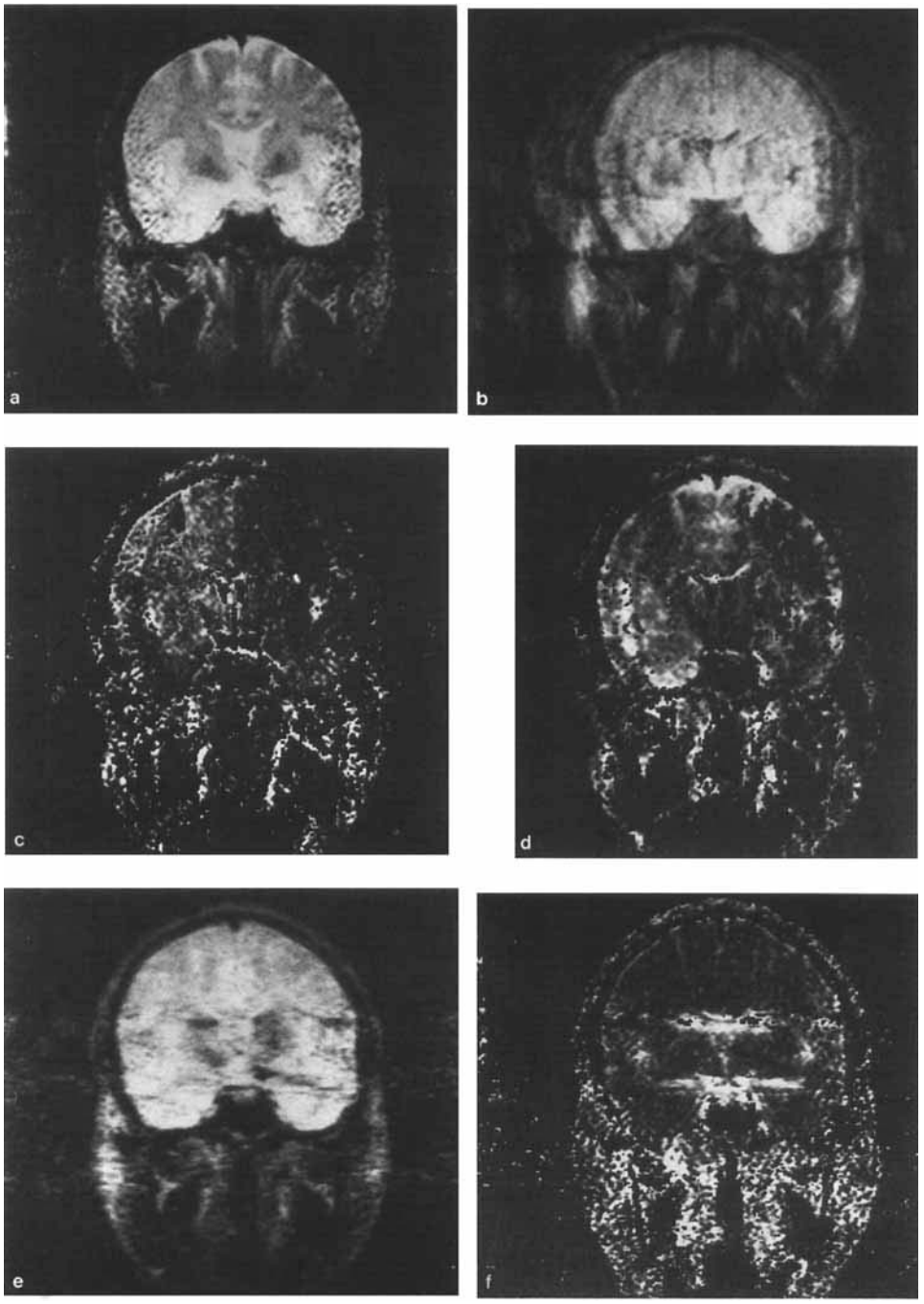

FIG. 4. Coronal images of the brain with cardiac gating acquired with (a) low motion sensitivity (i.e., *b*0) and (b) high motion sensitivity (i.e., *b*3) without phase correction. Calculated (c) perfusion and (d) diffusion images from non-phase-corrected data sets. (e) Phase-corrected version of the image in (b), and the corresponding calculated (f) perfusion and (g) diffusion images.

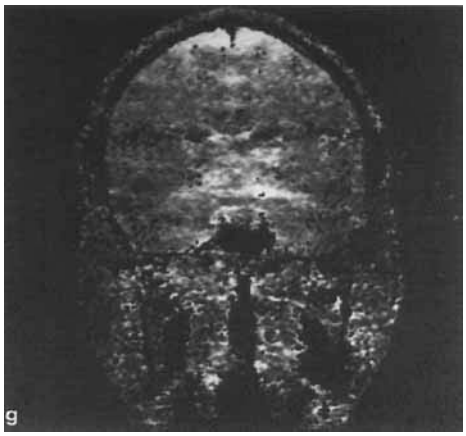

FIG. 4—*Continued*

Under such conditions, accurate quantification of incoherent motion properties is probably unrealistic. Nevertheless, note that the phase correction algorithm does allow differential attenuation of CSF and brain; however, the amount of CSF signal attenuation in the ventricles of Fig. 4e is underestimated. Non-phase-corrected images demonstrate near-complete CSF signal loss (apparent in less artifactual *b*1 and *b*2 images which are not shown), whereas the phase correction process fills in some CSF signal as dictated by the phase reference *b*0 image. The source of this error is the assumption that attenuation in image magnitude is constant for any given line in the phase encoding direction. This assumption is violated for CSF in the ventricles where the signal changes from intense signal, in the *b*0 image, to low signal in the motion-sensitive images, whereas the signal change of lateral brain tissue is far less dramatic. Near the top of the brain, CSF is contrasted against very little lateral tissue; consequently, the model of nearly uniform signal change along these phase encoding lines is appropriate, and the phase-corrected result more accurately displays high CSF attenuation.

These troublesome assumptions regarding permissible sources of phase change along the phase encoding direction are the motivation for the limited-volume acquisition approach. The images in Figs. 5a and b demonstrate location of a 10×10-mm column of tissue selected in the brain. The perfusion (Fig. 5c) and diffusion (Fig. 5d) images resulting from phase-corrected motion-sensitive images are informative for showing location and general perfusion/diffusion characteristics. However, when the column width is so limited and one assumes uniformity across this width as outlined above, then one essentially defines the object as one-dimensional. In such cases, we feel there is potentially greater value in one-dimensional quantitative plots of perfusion and diffusion values along the selected column axis in lieu of the gray-scale display. In addition, if one-dimensional plots are desired, then phase encoding and phase correction are not required since Fourier transformed echoes are combined in magnitude. Figure 6 is such an example for the tissue column shown in Fig. 5; these data sets were collected in a separate scan without phase encoding. Figs. 6a, b, and c display quan-

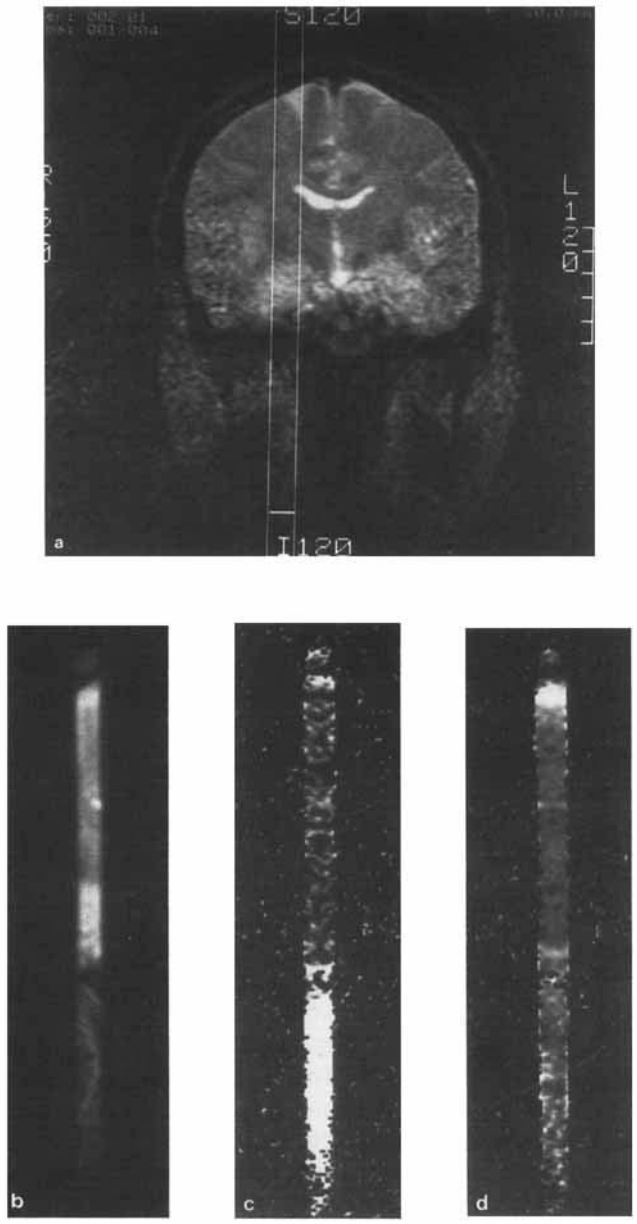

FIG. 5. Limited-volume acquisition of a 10 × 10-mm column in the brain without cardiac gating. (a) A full field-of-view motion-insensitive image showing location of prescribed column; (b) the actual column via orthogonal slice-selective gradients, *b*0 image; and (c) perfusion and (d) diffusion images calculated after phase correction.

titative plots of intensity (*b*0 data), perfusion, and diffusion respectively. The right-hand side of the plots in Fig. 6 correspond to the top of the tissue column in Fig. 5.

The data for Fig. 5 and 6 were collected without cardiac gating. The effect of cardiac

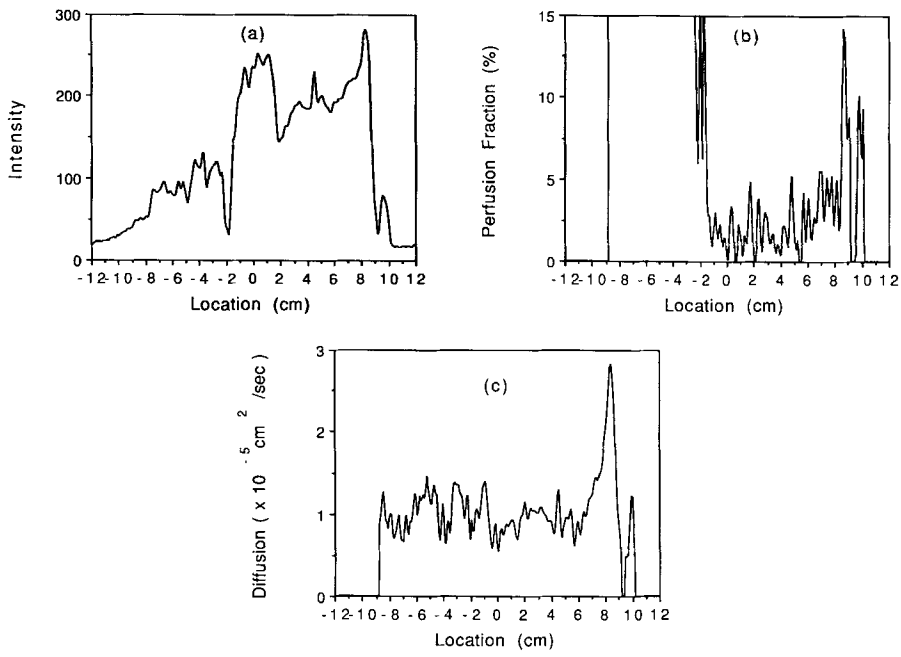

FIG. 6. Quantitative plots of incoherent motion properties of the tissue column shown in Fig. 5. (a) Intensity of signal ($b0$ data) along the column axis; calculated (b) perfusion fraction and (c) diffusion values. These data were collected without phase encoding or cardiac gating. Phase correction was not required since echoes were combined after 1D FT and magnitude calculation.

gating was investigated in limited-volume scans of another normal individual. The size and location of the column were similar to those shown in Fig. 5. The quantitative plots of signal intensity ($b0$ data), perfusion, and diffusion are in Figs. 7a, b, and c, with gated (solid) and nongated (dashed) results superimposed. Data from only the superior half of the column are displayed since it spanned the brain. The gated results display less spatial variability in perfusion values in the brain, but otherwise gated and nongated perfusion and diffusion values are in general agreement. Different TRs account for the reduced intensity of the nongated (TR = 1.5 s) data relative to the gated result (TR = 2 ECG cycles $\approx$ 1.8 s). Aside from variable saturation effects, we expect the gated and nongated results to be in close agreement, assuming perfusion flow signal attenuation is strong for $b1$, $b2$, and $b3$ acquisitions as modeled. For the $b1$ waveform of these experiments, perfusion flow attenuation is $F \leqslant 0.33$ (see Eq. [3]) for isotropic flow at $\geqslant 1$ mm/s. Variable inflow of unsaturated spins into the column may account for some of the discrepancy in gated versus nongated perfusion fraction results. Quantitative results from the region identified as predominantly white matter on images (location 5.3–8 cm) are perfusion fraction = 3.4 $\pm$ 1.1% and diffusion coefficient = 1.1 $\pm$ 0.2 $\times$ 10^{-5} cm^2/s for the gated data. Areas having more gray matter (1–4 and 8–9 cm) display higher perfusion and diffusion values. However, this may be due, in part, to partial volume averaging of CSF in these regions. These *in vivo* results are not verified by direct comparison with other experimental techniques; nevertheless, the perfusion fractions are in the realm of expected values of several

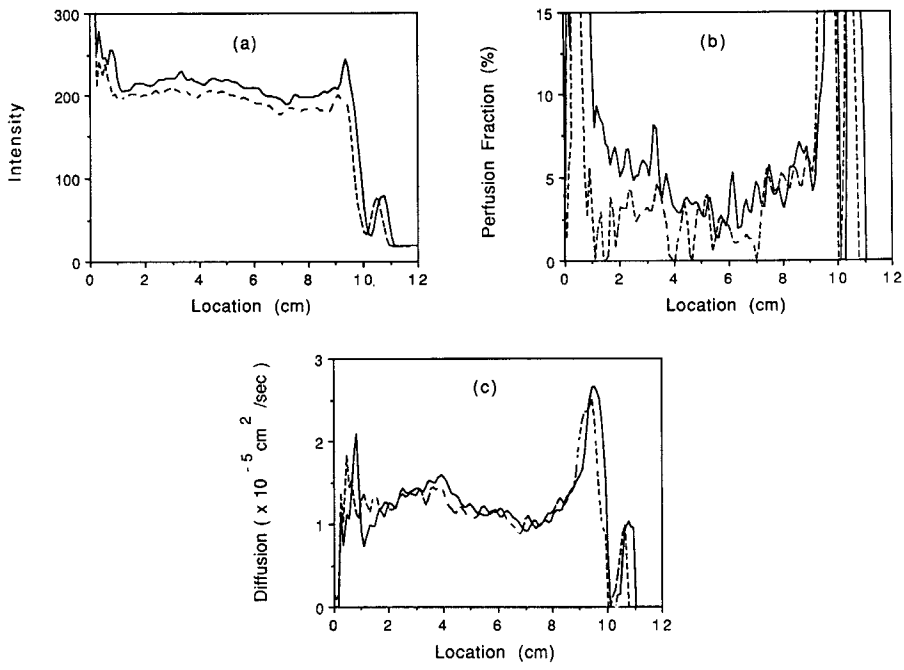

FIG. 7. Effect of cardiac gating on quantitative 1D perfusion and diffusion images of a 10 × 10-mm column in the brain. Cardiac-gated (solid line) and nongated (dashed line) results are superimposed in (a) intensity, (b) calculated perfusion fraction, and (c) diffusion value plots. Only the region of the column including the brain is plotted.

percent (*11*, *12*). We have applied the same acquisition and processing protocols to static acetone and water phantoms, however, yielding $D_{\text{acetone}} = 4.04 \pm 0.06 \times 10^{-5}$ cm^2/s, $f_{\text{acetone}} = 0.3 \pm 0.8\%$, and $D_{\text{water}} = 2.15 \pm 0.03 \times 10^{-5}$ cm^2/s, $f_{\text{water}} = 0.1 \pm 0.8\%$ at 21°C. The phantom diffusion results are in good agreement with the results of others (*3*).

In an effort to establish whether the calculated perfusion and diffusion values are truly related to desired physical processes, data from a column of tissue in the human calf were acquired while blood flow conditions were altered over an 18-min period as described above. Non-phase-encoded acquisition with interleaved b values allows temporally resolved calculation of perfusion and diffusion values. Figure 8 displays quantitative plots of perfusion (Fig. 8a) and diffusion (Fig. 8b) for three periods (3 min each): just before cuff inflation (normal flow), just before cuff deflation (low flow), and immediately after cuff deflation (reflow). Note there are pronounced changes in measured perfusion fraction dependent on flow, even in the area free of observable vessels (location > 0 cm), whereas diffusion remains nearly constant. The observations of constant diffusion with variable perfusion fraction are what one would predict if the calculated values are truly related to the targeted physical processes; consequently, these results are evidence in support of the validity of the method.

The elevated perfusion fraction after cuff release relative to the normal flow value is attributed to reactive hyperemia (*19*). The technique as currently applied does not, however, distinguish between increased perfusion due to greater blood volume and

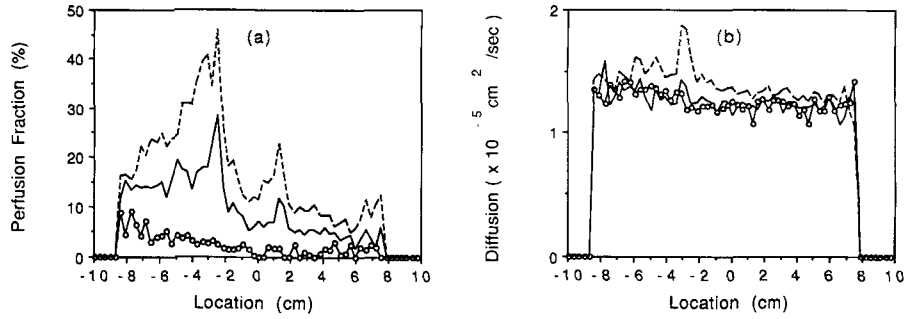

FIG. 8. Quantitative 1D images of perfusion and diffusion to human calf muscle where blood flow is altered by a pressure cuff on the thigh. (a) Perfusion fraction and (b) diffusion values along a 30 × 30-mm column muscle in the calf for normal flow before the cuff is inflated (solid), low flow 3–6 min after the cuff is inflated (dotted), and the reflow during the first 3 min after the cuff is released (dashed).

more rapid inflow of less saturated spins. Whichever the cause, the effect is undoubtedly blood flow related. The effect is most pronounced in the region of the large vessels (location < 0 cm), but is also observable in the region free of large vessels (location 2–6 cm) (perfusion fraction = 4.6 ± 1.1% precuff, 1.0 ± 0.9% cuffed, and 7.8 ± 1.5% postcuff).

CONCLUSIONS

MRI sequences designed for sensitivity to incoherent processes of perfusion and diffusion are known to be exceptionally sensitive to bulk tissue motion and to system instabilities, either of which may overwhelm incoherent effects. A conclusion of this work is that while cardiac gating provides some motion control, it alone is inadequate for quantitative IVIM imaging of the human brain. Results will vary dependent on patient, cardiac timing, and position in the brain; however, we expect that an unknown amount of artifact will exist in most cases. Phase-sensitive signal averaging may produce more appealing results, but does not prevent false attenuation from phase cancellation; consequently, perfusion/diffusion quantification accuracy remains compromised. Echo planar imaging may ultimately provide a solution to quantitative perfusion diffusion MRI by collecting a full phase-encoded data set with the body in one motion state (*20*), although currently this requires specialized hardware.

In this work, two methods were described which improve the feasibility of quantitative perfusion and diffusion measurement *in vivo*. The phase correction technique provides substantial image artifact reduction, but is inadequate by itself for use in human brain imaging. While coarse bulk motion and systematic phase errors are removed by the algorithm, there remains significant spatial variation in phase shifts and contrasts across the brain which is in violation of the algorithm model. This method, however, may have greater success in application to other parts of the body. Limited-volume acquisition is a simple modification designed to address the shortcomings of the phase correction approach by dividing the object into columns where the assumptions hold locally. Phase errors which vary temporally or spatially along the long axis of the column are remedied by the phase correction algorithm. Alternatively, phase encoding and correction can be omitted altogether to yield quantitative

one-dimensional images of perfusion and diffusion properties along the selected column. In this work, data from only one column were collected at a time; however, clearly more efficient schemes are possible using sequential or interleaved multicolumn acquisition. When phase encoding is not applied, the number of echoes collected from a given column is governed by signal to noise. Two-dimensional selective pulses (*15*) may benefit the limited-volume approach by reducing saturation cross-talk between selective volumes. An obvious drawback of selective excitation in lieu of phase encoding is loss of resolution in one dimension. We would like to emphasize, however, that this approach circumvents many of the major impediments to quantitative perfusion and diffusion measurement *in vivo*. To date numerous groups have investigated *in vivo* incoherent motion imaging in an experimental or clinical setting, yet there has been remarkably little consistent quantitative results given on diffusion coefficients. Data on perfusion via IVIM imaging is potentially more valuable, but is even more sparse. We expect that the above methods, if used alone or in comparison with two-dimensional techniques, may be beneficial toward quantitative incoherent motion measurement *in vivo*.

ACKNOWLEDGMENTS

This work was supported by General Electric Medical Systems, Milwaukee, Wisconsin, and the University of Michigan Department of Radiology.

REFERENCES

1. E. O. STEJSKAL AND J. E. TANNER, *J. Chem. Phys.* **42,** 288 (1964).
2. J. E. TANNER, *Biophys. J.* **28,** 107 (1979).
3. D. LE BIHAN, E. BRETON, D. LALLEMAND, M. L. AUBIN, J. VIGNAUD, AND M. LAVAL-JEANTET, *Radiology* **168,** 497 (1988).
4. K. D. MERBOLDT, H. BRUHN, J. FRAHM, M. L. GYNGELL, W. HÄNICKE, AND M. DEIMLING, *Magn. Reson. Med.* **9,** 423 (1989).
5. K-D. MERBOLDT, W. HÄNICKE, AND J. FRAHM, *J. Magn. Reson.* **64,** 479 (1985).
6. D. LE BIHAN, *Magn. Reson. Med.* **7,** 346 (1988).
7. S. PATZ AND R. C. HAWKES, *Magn. Reson. Med.* **4,** 140 (1986).
8. J. GEHRIG, R. BADER, H-J. ZABEL, P. BACHERT-BAUMANN, F. GÜCKEL, AND W. J. LORENZ, *in* "Proceedings, SMRM, 8th Annual Meeting, 1989," p. 135.
9. I. BERRY, C. MANELFE, P. CELSIS, AND J. P. MARC-VERGNES, *in* "Proceedings, SMRM, 8th Annual Meeting, 1989," p. 10.
10. R. L. COOPER, D. B. CHANG, A. C. YOUNG, C. J. MARTIN, AND B. ANCKER-JOHNSON, *Biophys. J.* **14,** 161 (1974).
11. G. PAWLIK, A. RACKL, AND R. J. BING, *Brain Res.* **208,** 35 (1981).
12. H. R. WEISS, E. BUCHWEITZ, T. J. MURTHA, AND M. AULETTA, *Circ. Res.* **51,** 494 (1982).
13. G. G. CLEVELAND, D. C. CHANG, C. F. HAZLEWOOD, AND H. E. RORSCHACH, *Biophys. J.* **16,** 1043 (1976).
14. P. R. MORAN, *Magn. Reson. Imaging* **1,** 197 (1982).
15. J. PAULY, D. NISHIMURA, AND A. MACOVSKI, *J. Magn. Reson.* **81,** 43 (1989).
16. L. AXEL, A. SHIMAKAWA, AND J. MACFALL, *Magn. Reson. Imaging* **4,** 199 (1986).
17. D. A. FEINBERG, AND A. S. MARK, *Radiology* **163,** 793 (1987).
18. M. E. MOSELEY, Y. COHEN, J. MINTOROVITCH, L. CHILEUITT, H. SHIMIZU, J. TSURUDA, D. NORMAN, AND P. WEINSTEIN, *in* "Proceedings, SMRM, 8th Annual Meeting, 1989," p. 136.
19. D. S. SUMNER, *in* "Vascular Surgery" (R. B. Rutherford, Ed.), p. 28, Saunders, Philadelphia, 1984.
20. R. TURNER, D. LE BIHAN, J. DELANNOY, AND J. PEKAR, *in* "Proceedings, SMRM, 8th Annual Meeting, 1989," p. 139.